J Mol Model (2019) 25: 206
https://doi.org/10.1007/s00894-019-4050-3

ORIGINAL PAPER

Single-walled carbon nanotubes in tetrahydrofuran solution: microsolvation from first-principles calculations

Mariana Kozlowska[1] · Bernd Meyer[2] · Pawel Rodziewicz[2,3]

Received: 11 February 2019 / Accepted: 24 April 2019 / Published online: 29 June 2019

Abstract

The molecular interactions between the commonly used solvent tetrahydrofuran (THF) and single-walled carbon nanotubes (SWCNT) are studied using density functional theory calculations and Car–Parrinello molecular dynamics simulations. The competitive interplay between THF–THF and THF–SWCNT interactions via C-H$\cdots$O and C-H$\cdots\pi$ hydrogen bonds is analyzed in detail. The binding energies for different global and local energy minima configurations of THF monomers, dimers, trimers, and tetramers on SWCNT(10,0) were determined. The adsorbed species are analyzed in terms of their coordination to the surface via weak hydrogen bonds of the C-H$\cdots\pi$ type and in terms of their ability to form intermolecular C-H$\cdots$O hydrogen bonds, which are responsible for the self-aggregation of THF molecules and a possible dimerization or tetramerization process. A special focus is put on the pseudorotation of the THF molecules at finite temperatures and on the formation of blue-shifting hydrogen bonds.

Keywords Microsolvation · Tetrahydrofuran · Carbon nanotubes · DFT · CP-MD

Introduction

Carbon nanotubes (CNTs) are quasi one-dimensional objects with interesting properties such as a high surface area, tunable electronic band gap, and high thermal conductivity [1]. The extraordinary mechanical and electrical properties of CNTs make them a potentially useful material for nanotechnology, electronics, and optics [2–4]. One of the main limitations for future applications of CNTs in industry is their inherent low solubility [5]. This makes it difficult to disperse the CNTs, which is a pre-requirement for the practical use of CNTs as a nanomaterial. The choice of solvent for obtaining well-dispersed particles in either aqueous or organic media is a challenging task [6]. Furthermore, the majority of chemical reactions take place in solution. For CNT functionalization, it is therefore crucial to find appropriate solvents that allow achieving a satisfactory chemical yield and simultaneously are able to disperse the carbon nanotubes.

The solvation process depends on the interplay between CNT–solvent and solvent–solvent interactions. Therefore, CNT dispersions of differently sized tubes have to be treated as locally microsolvated systems on the molecular level. The extended π-electron system of the CNTs is responsible for a crucial part of the CNT–solvent interaction, since the π-electron density acts as a proton acceptor in a process of H-bond formation. Many different types of A-H$\cdots\pi$ hydrogen bonds with respect to the A-H proton donor and the H-bond strength were described in the literature up to now [7]. One of the most common and most abundant interactions of this type in organic chemistry are weak C-H$\cdots\pi$ hydrogen bonds [8]. The formation of an H-bond between an A-H proton donor and a B-Y proton acceptor (where A is an electronegative atom and B is either an electronegative atom or a group with regions of high electron density) is typically accompanied by an

This paper belongs to the Topical Collection Tim Clark 70th Birthday Festschrift

Dedicated to Tim Clark on the occasion of his 70th birthday

✉ Pawel Rodziewicz
pawel.rodziewicz@fau.de

[1] Institute of Nanotechnology, Karlsruhe Institute of Technology (KIT), Hermann-von-Helmholtz-Platz 1, 76344 Eggenstein-Leopoldshafen, Germany

[2] Interdisciplinary Center for Molecular Materials (ICMM) and Computer-Chemistry-Center (CCC), Friedrich-Alexander-Universität Erlangen-Nürnberg (FAU), Nägelsbachstr. 25, 91052 Erlangen, Germany

[3] Institute of Chemistry, Jan Kochanowski University, Swietokrzyska Str. 15G, 25-406 Kielce, Poland

elongation of the A-H bond, causing a red shift of the A-H stretching frequency and a substantial increase of the IR integral intensity of the A-H bands compared to the non-interacting species [7, 9, 10]. These changes are observed for the majority of H-bonded molecular systems and are frequently used in literature as a definition for the presence of a hydrogen bond. However, many of the C-H$\cdots$O and the C-H$\cdots\pi$ hydrogen bonds reveal exactly opposite features, namely a shortening of the A-H bond, a considerable blue shift of the A-H stretching frequency and a decrease of the integral intensity of this band [11–14].

Tetrahydrofuran (THF) is a commonly used solvent for carbon nanotubes [1, 4, 15]. Its low boiling point enables easy removal of the THF molecules from the reaction mixture. The weak intermolecular interactions in THF originate from a network of weak C-H$\cdots$O hydrogen bonds. Recently, tetrahydrofuran was also used as anchoring agent in the synthesis of uniformly distributed Pt and PtSn nanoparticles on THF-functionalized CNTs [16]. Electrocatalytic activity in fuel cells was demonstrated for the CNT-supported particles. The initial arrangement of the THF molecules on the CNT surfaces was crucial for achieving a high reaction yield and a uniform distribution of the Pt and PtSn nanoparticles [16].

The tetrahydrofuran molecule can easily change its conformation due to the high flexibility of its five-membered ring [17]. The process of changing the conformation is observed in experiment and is called pseudorotation [17–21]. High-level ab initio calculations show that the global minimum of the THF molecule in the gas phase is an envelope structure with C_s symmetry [20–22]. According to the latest coupled-cluster CCSD(T) benchmark calculations the absolute energy difference between the global minimum (C_s) and the first local minimum, the twisted conformation (with C_2 symmetry), is only 0.59 kJ mol^{-1} [22]. These theoretical findings were also confirmed by electron momentum spectroscopy (EMS) experiments supported by density functional theory calculations [23]. Such a low difference between the global and the local minima suggest a high flexibility of the THF molecule at finite temperatures and an ability to adapt barrierless to different adsorption sites.

The THF molecules in the solvent mainly interact via C-H$\cdots$O hydrogen bonds, where the THF molecules are simultaneously both proton donor and acceptor. The oxygen atom of the THF molecules might also accept two C-H$\cdots$O hydrogen bonds. Such structures were observed in theoretical simulations of liquid THF [24, 25]. The C-H$\cdots$O hydrogen bonds are particularly important in large molecular networks where cooperative effects stabilize the system [26, 27]. In the microsolvation of CNTs the solvent–solvent attractive forces are counterbalanced by CNT–solvent interactions. In the case of a THF environment, the main contributions originate from weak directional C-H$\cdots\pi$ hydrogen bonds and rather isotropic dispersion forces. These types of interactions are predominant in the stabilization of many biological systems [28–31].

The aim of this study is a detailed characterization of the interplay between CNT–solvent and solvent–solvent interactions and in particular the nature of the C-H$\cdots\pi$ and C-H$\cdots$O hydrogen bonds. We use a combination of mutually supplemental computational approaches, namely density functional theory (DFT) geometry optimizations and Car–Parrinello molecular dynamics (CP-MD) simulations, to study the structural properties of THF molecules on the surface of a single-walled carbon nanotube (SWCNT). As a model for our theoretical studies, we have chosen the SWCNT(10,0) since it is one of the most stable and abundant single-walled carbon nanotubes [32]. The microsolvation of the carbon nanotubes is modeled by decorating the SWCNT(10,0) surface with THF molecules and by increasing stepwise the surface coverage from one to four THF molecules within our periodic supercell. For simplicity, these configurations will be called a monomer, dimer, trimer, and tetramer on the SWCNT(10,0) surface, although this notation, in the first place, refers to the number of THF molecules in one SWCNT supercell (the surface coverage) and does not strictly imply a cluster of this size. Configurations where two and more THF molecules form aggregates will be discussed specifically in the text. For the different surface coverages, we analyze binding energies and structural parameters of the global and local minima configurations. Specifically, we will focus on the structural flexibility of the molecules at finite temperature, in particular the pseudorotation, and on the formation of blue-shifting hydrogen bonds.

Computational methods

All calculations were performed within the framework of density functional theory (DFT) using periodic boundary conditions. Equilibrium geometries of THF monomer, dimer, trimer, and tetramer configurations on the surface of a (10,0) SWCNT were obtained using the PWscf code from the Quantum ESPRESSO package [33]. Exchange and correlation effects were described by the gradient-corrected functional of Perdew, Burke, and Ernzerhof (PBE) [34]. The ionic cores were represented by Vanderbilt ultrasoft pseudopotentials [35]. A plane-wave basis set truncated at 30 Ry was employed to expand the electronic wave functions. Due to the large size of the supercell, k-point sampling could be restrict to the Γ-point. Test calculations for the minimum structure of THF monomers on SWCNT(10,0) showed that increasing the k-point density by using a $1 \times 1 \times 4$ Monkhorst-Pack k-point

mesh changes the absolute THF binding energy by less than 0.3 kJ mol^{-1} (energy differences between local energy minima are even less affected).

The geometry optimizations were done without any constraint. The empirical D2 dispersion correction proposed by Grimme was included to describe van der Waals interactions [36]. The initial atomic positions of a (10,0) SWCNT were generated using the TubeGen program [37]. The tube was placed into a tetragonal supercell with dimensions of $a = b = 20.0$ Å and $c = 17.1394$ Å. The length of the c-axis was obtained by performing geometry optimizations for a set of 12 c values and by determining the energy minimum from a polynomial fit to the data points.

The first-principles molecular dynamics simulations were performed by using the Car–Parrinello approach [38] as implemented in the CPMD program [39]. Systems with four THF molecules deposited on the SWCNT(10,0) surface were simulated using periodic boundary conditions at a temperature of 300 K, which mimics the interaction of THF molecules and CNTs in the microsolvation process. A time step of 4 a.u. and a fictitious electronic mass of 400 a.u. were applied. The temperature was imposed by Nosé–Hoover chain thermostats for the nuclear degrees of freedom with a coupling frequency of 1600 cm^{-1} [40, 41]. The infrared spectrum of carbon nanotubes shows an intense peak in the region of 1500–1600 cm^{-1}. Our choice for the coupling frequency therefore enables an efficient coupling between the thermostats and the vibrational degrees of the simulated SWCNT. The final temperature of the simulation was achieved by increasing stepwise the temperature from 0 K to 300 K in steps of 50 K. The system was equilibrated at 300 K for 1 ps before accumulating statistics in a production run of 10 ps. The total Hamiltonian energy in the production run had a very small drift of about 0.0002 a.u., which is significantly below the threshold recommended by VandeVondele et al. [42]. All other settings in the CP-MD simulations (exchange-correlation functional, pseudopotentials, plane wave energy cutoff, k-points and supercell size) were the same as in the static DFT calculations.

Results and discussion

Tetrahydrofuran molecule

Theoretical studies of molecular interactions in large periodic systems, as in the case of THF microsolvation of carbon nanotubes, require reliable but computationally not too demanding approaches. DFT within a plane wave basis set framework offers a very good compromise between accuracy and computational cost. A comparison of the structural and energetic parameters for the isolated THF molecule between DFT calculations with common gradient-corrected functionals [22, 23] and high level ab initio methods [20–22] confirms that DFT gives a satisfactory precision for the description of the different conformers. Calculations utilizing hybrid functionals (B3LYP and PBE0) and D3 dispersion corrections, in contrast, wrongly predict the twisted (C_2) THF conformation as the global minimum [22].

Our calculations based on DFT/PBE+D2, pseudopotentials, and a plane-wave basis set correctly predict the global minimum structure as the envelope (C_s) configuration. The energy difference between the envelope (C_s) and the twisted (C_2) conformation is 1.27 kJ mol^{-1}, which is in very good agreement with the result of 0.59 kJ mol^{-1} obtained from high-level ab initio CCSD(T) calculations [22]. Weak C-H$\cdots\pi$ and C-H$\cdots$O hydrogen bonds, the crucial interactions for the microsolvation of CNTs in THF, are both known to show unusual spectroscopic properties. Our previous calculations on weakly H-bonded complexes showed that the blue-shifting phenomenon is also properly described by our DFT/PBE approach [43–46].

The strength of the interactions between THF and the carbon nanotubes depends on the ability of the reactants to change their conformation in the process of complex formation. CNTs cannot undergo conformational changes so they can be treated as rigid molecules. In contrast, the THF molecule can adjust to the substrate by undergoing a conformational change known as pseudorotation [17–21]. Since the gas phase energy difference between the global energy minimum structure C_s and the twisted C_2 conformation is so small, the THF molecule will automatically adopt its preferred conformation in the geometry optimization when it is placed on the SWCNT surface. In our calculations, we therefore always started from the C_s structure of the THF molecule as the initial geometry. In the majority of the analyzed systems, the C_s conformation remained unchanged. However, when THF molecules start to aggregate we indeed see conformational changes. These cases will be discussed specifically in the next subsections.

The chosen (10,0) single-walled carbon nanotube has a relatively large diameter so that the largest analyzed THF aggregate consisting of four THF molecules may be still considered an isolated tetramer. In addition, the length of the c-axis of the supercell prevents the interaction of the THF tetramer with its periodic image.

Adsorption of THF monomers on SWCNT(10,0)

The THF molecule has the same structural skeleton as furan. However, the presence of additional hydrogen atoms prevents planarity of THF, contrary to the aromatic furan molecule. Thus, the intermolecular interactions between

THF and SWCNT are not based on π–π stacking but mainly on C-H$\cdots\pi$ hydrogen bonds. Among all types of C-H$\cdots\pi$ hydrogen bonds where the proton acceptor is a region of high electron density, the H-bonds to π electrons are one of the strongest. Methane adsorbed on the surface of a SWCNT is the prototype of a structure, which is governed by C-H$\cdots\pi$ hydrogen bonds. Woods et al. report the hollow site to be the global minimum of CH_4 on SWCNT(8,0) with a binding energy of 9.17 kJ mol^{-1} [47]. The other positions of the CH_4 molecule on the surface of SWCNT(8,0), namely top and bridge, have binding energies of 8.10 and 7.72 kJ mol^{-1}, respectively.

In the case of a single THF molecule in contact with a SWCNT(10,0) surface, up to four C-H$\cdots\pi$ hydrogen bonds might be formed. In the gas phase global minimum structure of the THF molecule (C_s), all H atoms on both sides of the carbon skeleton are equiplanar. Thus, if the plane of the THF molecule marked by the carbon skeleton is parallel to the SWCNT surface, four C-H can act as a proton donor in the formation of C-H$\cdots\pi$ hydrogen bonds. The adsorbate structure is rigid, but the THF molecule can slightly adjust its conformation. The pseudorotation of the THF skeleton can not change significantly the position of the H atoms. So in good approximation, we can treat the adsorption of THF on the SWCNT(10,0) surface as the interaction of two rigid species. However, since no constraints are imposed in the geometry optimization, the conformation of THF may change to the twisted C_2 configuration, and such flips are observed in the case of the THF trimer and tetramer.

The binding energy of the THF molecule adsorbed on the carbon nanotube in different configurations depends on the number of C-H groups actually involved in C-H$\cdots\pi$ bonds and on the lateral position of the molecule on the surface (bridge, top or hollow). Altogether, we analyzed 16 different positions of the THF molecule on the SWCNT(10,0) surface by a systematic choice of initial lateral displacements. The initial configuration of the THF molecules was always its global minimum structure C_s in the gas phase. Figure 1 shows selected optimized geometries of eight THF/SWCNT(10,0) structures labeled **A**–**H**. The calculated binding energies of the global minimum **A** (−29.1 kJ mol^{-1}) and the first local minimum structure **B** (−28.8 kJ mol^{-1}) are very similar, but their bonding patterns are significantly different. We report all binding energies with a precision of one decimal place in order to distinguish different configurations, without the intention to suggest that this is the accuracy of our PBE+D2 setup.

The structure **A** and **B** have the same arrangement of the oxygen atom with respect to the surface of the SWCNT(10,0). The orthographic projection of THF/SWCNT(10,0) along the axis perpendicular to the plane spanned by the carbon skeleton of the THF molecule, shown in Fig. 1, indicates that the oxygen atom is in the center of a tube hexagon. The distance R(O$\cdots$C) between

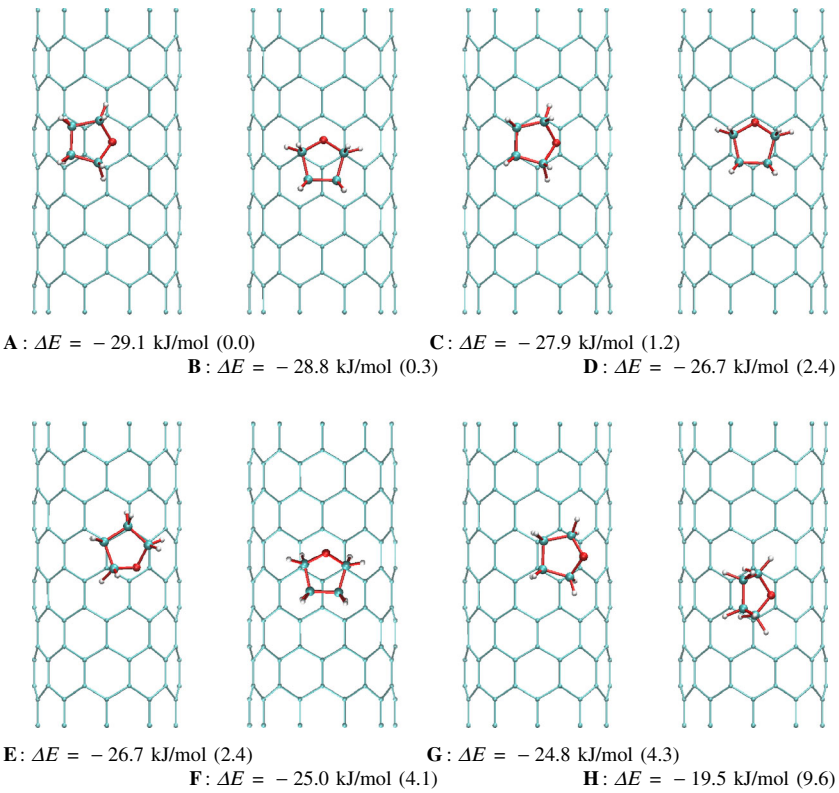

Fig. 1 Global and local minima structures of THF monomers on SWCNT(10,0). The relative binding energies are calculated with respect to the global minimum and are given in parenthesis

the oxygen atom from THF and the closest carbon atom from SWCNT(10,0) is 3.2202 and 3.1136 Å for the structure **A** and **B**, respectively. The global minimum **A** can be obtained from the first local minimum **B** by rotating the THF molecule by 90° with respect to the surface normal of the carbon nanotube (see Fig. 1). We therefore label the structure **A** and **B** as *transverse* and *parallel*, respectively.

Even though the binding energies of the global minimum (**A**) and the first local minimum (**B**) are almost identical, they represent a different bonding pattern with respect to the structural parameters of the C-H$\cdots\pi$ hydrogen bonds. Table 1 collects the calculated distances R(H$\cdots$C) between the H atoms and their closest C atom from the surface of the carbon nanotube. The corresponding C-H bond lengths r(C-H) of all considered C-H$\cdots\pi$ hydrogen bonds are also presented. Each THF molecule interacts with the SWCNT(10,0) surface via four C-H$\cdots\pi$ hydrogen bonds. Their structural parameters are listed in Table 1 in clockwise order starting from the first carbon atom after the oxygen atom. The CH_2 group located next to the oxygen atom is known as αCH_2, whereas the second one is called βCH_2. In addition, Table 1 shows the values of the difference Δr(C-H) between the C-H distance in the THF molecule on the surface and the C-H bond length calculated for the isolated THF molecule in the gas phase. The observed contraction or elongation of the C-H bond is denoted as a negative or positive value of Δr(C-H), respectively.

The character of the H-bond in THF/SWCNT(10,0) is determined by the sign of Δr(C-H): a positive value refers to a conventional H-bond, whereas a negative sign indicates an improper, blue-shifting, H-bond. Well-established correlations between the change of the C-H bond length and the shift of the ν(CH) stretching vibration can be found in the literature [46, 48–50]. In our case, the spectroscopic manifestation of the C-H$\cdots\pi$ hydrogen bond formation in structure **A** and **B** can be estimated to be rather weak, since the changes in the C-H bond length are very small, ranging from −0.0003 to 0.0007 Å, see Δr(C-H) in Table 1. For the global minimum **A**, we can expect a blue shift of the order of several cm^{-1} for the symmetric $\nu(\alpha CH_2)$ stretching vibration. Since the full vibrational analysis for a system of the size of THF/SWCNT(10,0) is computationally a very demanding task, we performed a frequency calculation only for structure **A**. The result confirms the mentioned prediction for the vibrational shift from above. For the symmetric $\nu(\alpha CH_2)$ stretching vibration of the THF molecule in global minimum **A**, we find a blue shift of only 6 cm^{-1}. While for the THF monomer the changes in the C-H bond length Δr(C-H) and thus the shifts in the C-H stretching vibration are rather small, we will see larger values for the THF dimer, trimer, and tetramer due to the additional interactions via C-H$\cdots$O hydrogen bonds.

Apart from correlating structural parameters to spectroscopic properties of the proton donor, one can also estimate the strength of the C-H$\cdots\pi$ hydrogen bonds by comparing the H$\cdots$C distances (see Table 1). For both structures **A** and **B**, the values of the respective H$\cdots$C distances do not differ

Table 1 Structural parameters of a THF monomer adsorbed on SWCNT(10,0)

	THF monomer							
Label	**A**	**B**	**C**	**D**	**E**	**F**	**G**	**H**
ΔE	−29.1	−28.8	−27.9	−26.7	−26.7	−25.0	−24.8	−19.5
R(O$\cdots$C)	3.2202	3.1136	3.1186	2.9310	3.0402	4.3297	4.6434	3.3829
R(H$\cdots$C)	2.8435	3.0616	2.8896	3.1378	3.0300	2.7685	2.6105	2.7383
	2.7160	2.7376	2.7530	2.7734	2.7442	2.7700	2.6407	5.1125
	2.7075	2.7540	2.7521	2.7762	2.8231	2.7506	2.6447	4.9709
	2.8457	3.0108	2.8924	3.0364	3.1820	2.7840	2.6224	2.7044
r(C–H)	1.0997	1.1002	1.1002	1.1007	1.1007	1.1092	1.1095	1.0998
Δr(C–H)	0.0002	0.0007	0.0007	0.0012	0.0012	0.0097	0.0100	0.0003
r(C–H)	1.0994	1.0992	1.0998	1.0993	1.0993	1.1001	1.1000	1.0998
Δr(C–H)	−0.0001	−0.0003	0.0003	−0.0002	−0.0002	0.0006	0.0005	0.0003
r(C–H)	1.0993	1.0995	1.0997	1.0996	1.0990	1.0998	1.1001	1.0992
Δr(C–H)	−0.0002	0.0000	0.0002	0.0001	−0.0005	0.0003	0.0006	−0.0003
r(C–H)	1.0998	1.1002	1.1001	1.1005	1.1005	1.1095	1.1098	1.0998
Δr(C–H)	0.0003	0.0007	0.0006	0.0010	0.0010	0.0100	0.0103	0.0003

Bond lengths and binding energies ΔE are given in Å and kJ/mol, respectively. R(O$\cdots$C) is the distance between the O atom from THF and the closest C atom from the SWCNT. The C-H$\cdots\pi$ hydrogen bonds are characterized by the R(H$\cdots$C) distance between the H atom and the closest SWCNT carbon atom as well as the C-H bond length r(C-H) and its change with respect to the gas phase structure Δr(C-H)

by more than 0.2 Å. So the strength of the C-H$\cdots\pi$ bonds might be averaged and the strength of a single bond is given by one-fourth of the binding energy, i.e., about 7 kJ mol^{-1}. This is a typical value for such a type of interaction and it is comparable to the results obtained for the binding energy of methane on a SWCNT [47].

The binding energy of the next local minimum structure **C** is −27.9 kJ mol^{-1}, i.e., it is less stable than the global minimum by 1.2 kJ mol^{-1}. The bonding pattern of **C** can be described as a translation of the THF molecule from the global minimum **A** in the direction perpendicular to the CNT axis by half of a tube hexagon. Figure 1 shows that the oxygen atom is now over a C–C bond. The calculated O$\cdots$C distance (see Table 1) is almost identical as in the structures **A** and **B**. The hydrogen bonding pattern is also similar to the global minimum. All values of the H$\cdots$C distance do not differ by more than 0.1 Å with respect to those for structure **A**. The lower stability of the structure **C** in comparison to the global minimum **A** might be thus attributed to the position of the oxygen atom.

A similar scenario is observed for structure **D** where the binding energy is lower by 2.4 kJ mol^{-1} than for the global minimum. Structure **D** can be described as a translation of the THF molecule from the first local minimum **B** in the direction parallel to the CNT axis by half of a tube hexagon. The oxygen atom is now located over a carbon atom with an O$\cdots$C distance of 2.9310 Å. In the local minimum **E**, the oxygen atom has a position close to a C–C bond on the surface, (see Fig. 1), and the binding energy is identical to structure **D**. The calculated H$\cdots$C distances for structure **D** and **E** show a similar trend, where the hydrogen atoms from αCH_2 groups form weaker C-H$\cdots\pi$ hydrogen bonds than those from the βCH_2 groups (see Table 1).

The analysis of the structural differences between the local minima **A**–**E** shows that the THF binding energy is determined by the interplay between the C-H$\cdots\pi$ hydrogen bonds and the O$\cdots\pi$ interactions. The THF molecule in its envelope configuration C_s can have two orientations on the SWCNT surface: with the oxygen atom up or down with respect to the plane spanned by the carbon skeleton. In the structures **A**–**E** analyzed so far, the oxygen atom was closer to the surface (down orientation). As a result, the O$\cdots\pi$ interactions slightly push the THF molecule away from the surface and make the two αC-H$\cdots$C distances longer than the βC-H$\cdots$C ones.

The influence of the interaction between the oxygen atom from the THF molecule and the π electronic density on the surface becomes clearly visible in structure **F**. In structure **F**, the THF molecule adopts the preferred envelop configuration (C_s), but the oxygen atom is up with respect to the plane spanned by the carbon skeleton and its distance to the closest carbon atom from the surface is 4.3297 Å. Such an arrangement of the THF molecule reduces the influence of the O$\cdots\pi$ interactions on the binding energy. The structure has a very similar C-H$\cdots\pi$ bonding pattern as the first local minimum **B**, however it is less stable by 3.8 kJ mol^{-1}. All values of the H$\cdots$C distance calculated for structure **F** are lower than 2.8 Å, so the reduction of the O$\cdots\pi$ interactions enables closer contact between the THF and the SWCNT via slightly stronger C-H$\cdots\pi$ hydrogen bonds.

We observe a similar situation for structure **G**. Here, the H$\cdots$C distances are the shortest among the all global and local minima for THF monomers, dimers, trimers, and tetramers, and they do not exceed 2.65 Å (see Table 1). Structure **G** and **C** have a very similar C-H$\cdots\pi$ bonding pattern. The binding energy of structure **G** is −24.8 kJ mol^{-1} and it is less stable by 3.1 kJ mol^{-1} than the structure **C**. The O$\cdots\pi$ interactions are significantly reduced due to a large O$\cdots$C distance of 4.6434 Å.

In the structures **A**–**G**, the plane spanned by the THF carbon atoms was always oriented parallel to the SWCNT surface so that both α and βCH_2 groups could form simultaneously C-H$\cdots\pi$ hydrogen bonds to the nanotube. In our study, we also considered structures where the THF molecule interacts with the SWCNT only with its αCH_2 groups. Structure **H** has been selected as a representative example from the local minima with such a type of arrangement of the THF molecule on the surface. It is the least stable local minimum among all considered monomer structures and its binding energy is only −19.5 kJ mol^{-1}. In addition to its two αC-H$\cdots\pi$ hydrogen bonds, the THF molecule only interacts via a O$\cdots\pi$ contact with the nanotube surface. We therefore consider structure **H** to be rather unstable at finite temperatures, however, similar hydrogen bonding motifs were observed in our Car–Parrinello molecular dynamics simulations (see Adsorption of THF tetramers on SWCNT(10,0)).

Adsorption of THF dimers on SWCNT(10,0)

The next step in our analysis of the interplay between CNT–solvent and solvent–solvent interactions is to study THF dimers on the SWCNT(10,0) surface. The contribution from THF–THF interactions to the overall binding energy of THF dimers on the SWCNT(10,0) surface can be estimated on the basis of results from calculations for the THF dimer in the gas phase. High-level ab initio calculations on the CCSD(T) level show that the most stable THF dimer sandwich-like configuration is stabilized by two C-H$\cdots$O hydrogen bonds with a dissociation energy of 19.0 kJ mol^{-1} [22]. In this structure, both THF molecules adopt their global minimum envelop conformation (C_s), however, other dimer configurations of the THF molecules were also considered. For example, the THF dimer where both molecules have the twisted conformation C_2 is less stable by 2.7 kJ mol^{-1} than the global optimum [22].

In our study of THF dimers on the SWCNT surface, we focus again, as in the case of the monomers, on structures were the THF molecules are in their global minimum envelop conformation. On the basis of the obtained results for the THF monomer, we considered different initial configurations for the THF dimers on the surface. As we have seen for the monomer, the binding energy does not depend significantly on the position of the adsorbent molecule. Therefore, we focus in our analysis only on two THF dimer structures with *parallel* (**A**) and *transverse* (**B**) orientation with respect to the axis of the carbon nanotube.

The binding energy of the global minimum **A** of the THF dimer is -64.3 kJ mol^{-1} and its structure is presented in Fig. 2. The binding energy of the global optimum of the THF monomer is -29.1 kJ mol^{-1}, so the gain in the binding energy for the most stable THF dimer due to the formation of two C-H$\cdots$O H-bonds is 6.1 kJ mol^{-1}. This value is much lower than the one obtained from the calculations for the THF dimer in the gas phase [22]. This is not surprising, since in the gas phase the THF dimer can adapt to the most stable configuration without any geometric constraints. On the other hand, on the carbon nanotube the THF dimer has to rearrange due to the interactions with the surface. Here, the interplay between C-H$\cdots$O hydrogen bonds in the THF dimer and the C-H$\cdots\pi$ interaction with the surface has to be optimized. In the gas phase, the C-H$\cdots$O hydrogen bonds lead to a sandwich-like structure for the THF dimer as the global minimum, whereas in the case of the THF dimer on the carbon nanotube the THF molecules maximize the interactions with the surface via eight C-H$\cdots\pi$ H-bonds (see Fig. 2 and Table 2).

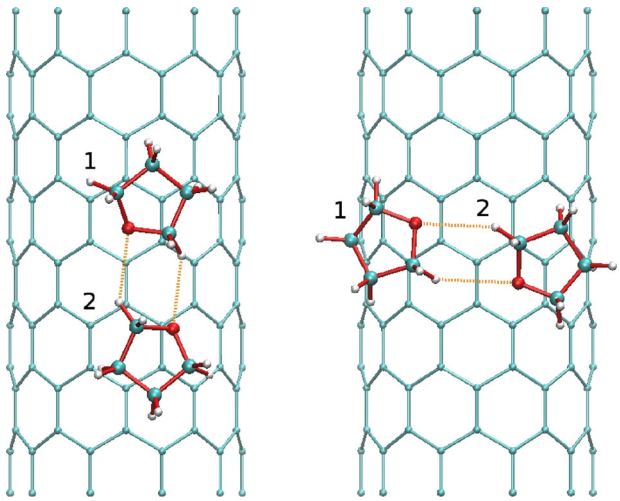

A : ΔE = − 64.3 kJ/mol (0.0) **B** : ΔE = − 61.8 kJ/mol (2.5)

Fig. 2 Global and local minima structures of THF dimers on SWCNT(10,0). The THF–THF interactions via C-H$\cdots$O hydrogen bonds are marked by *dashed lines*. THF molecules are numbered for assignment of their structural parameters in Table 2. The relative binding energies are calculated with respect to the global minimum and are given in parenthesis

The C-H$\cdots$O hydrogen bonds are well-known examples for the phenomena of blue-shifting H-bonds, where the C-H bond length shortens and a blue shift of the stretching vibration occurs [51, 52]. In structure **A**, we observe a contraction of the C-H bond involved in the C-H$\cdots$O hydrogen bonds of Δr(C–H) = -0.0003 Å and -0.0010 Å (see Table 2). According to the well-established correlation between Δr(C–H) and $\Delta\nu$(C–H) mentioned in "Adsorption of THF monomers on SWCNT(10,0)", the estimated value of the blue shift is of the order of 12 cm^{-1}. The intermolecular distances H$\cdots$O are 2.5309 and 2.5649 Å, which are a typical values for the C-H$\cdots$O hydrogen bonds [46].

The *transverse* structure **B** is less stable in comparison to the global minimum **A**. Both H$\cdots$O distances are elongated to 2.7298 and 2.8468 Å. The THF molecules wrap around the carbon nanotube to maximize their interactions with the surface via the creation of eight C-H$\cdots\pi$ hydrogen bonds, which weakens the mutual C-H$\cdots$O THF–THF interactions. The O$\cdots$C distances (see Table 2) for the dimer **A** and **B** are almost identical, so the curvature of the nanotube mostly influences the THF–THF interactions rather than the THF–SWCNT bonding of the individual THF molecules.

Adsorption of THF trimers on SWCNT(10,0)

In the THF dimers, each THF molecule was simultaneously a proton donor and a proton acceptor. However, a THF molecule can accept two or more C-H$\cdots$O hydrogen bonds via its lone electron pairs at the oxygen atom. Therefore, it is possible to form larger THF aggregates than a dimer. In this section we consider trimers with three THF molecules on the SWCNT(10,0) surface. Figure 3 shows two structures, the global minimum **A** obtained from an initial *parallel* arrangement of the THF molecules, which indeed remains a THF trimer cluster, and structure **B** with a THF dimer on one side and the third THF molecule of the initial *transverse* orientation of the trimer has split-off and moved to the other side of the nanotube.

The global minimum **A** is a THF aggregate with a network of four C-H$\cdots$O hydrogen bonds with an overall binding energy of -92.6 kJ mol^{-1}. The molecules with the number 1 and 2 form the dimer motif known from the previous section (see Fig. 3). We observe here also a bifurcated C-H$\cdots$O hydrogen bond originating from THF molecule number 2. The oxygen atom of the additional third THF molecule acts as a proton acceptor for two C-H$\cdots$O hydrogen bonds. However, the dimer motif differs from the global minimum structure discussed in the previous section, namely, the molecule number 2 has adopted the twisted

Table 2 Structural parameters of a THF dimer, trimer and tetramer adsorbed on SWCNT(10,0)

	THF dimer		THF trimer		THF tetramer	
Label	**A**	**B**	**A**	**B**	**A**	**B**
ΔE	−64.3	−61.8	−92.6	−88.9	−145.4	−129.6
R(O···C)	3.1245	3.1402	3.1375	3.1525	3.1730	3.1308
	3.1143	3.1090	3.1627	3.1266	3.0285	3.1505
	–	–	3.1365	3.0868	3.1726	3.1955
	–	–	–	–	3.1194	3.1612
R(H···O)	2.5309	2.7298	2.7226	2.7453	2.4932	2.5871
	2.5649	2.8468	2.7466	2.5160	2.4624	2.5908
	–	–	2.4907	–	2.6528	2.6092
	–	–	2.8888	–	2.4209	2.5347
R(H···C)	3.2700	2.9820	2.9499	2.7560	3.0103	3.2047
THF No. 1	2.7952	2.7077	2.7427	3.1581	2.7997	2.6879
	2.6690	2.7715	2.8113	2.6663	2.7629	2.7244
	2.8967	2.9941	3.1020	3.0295	2.7888	2.8735
R(H···C)	3.0544	2.8652	2.7425	2.9542	2.7071	3.2268
THF No. 2	2.7753	2.9135	4.5328	2.7256	4.0596	2.6191
	2.7434	2.6775	2.7143	2.7856	2.7946	2.7088
	3.2029	3.1046	2.9809	3.0955	2.9577	2.8000
R(H···C)	–	–	3.2586	3.1496	2.7555	3.2302
THF No. 3	–	–	2.6802	2.6546	2.9739	2.7104
	–	–	2.8429	2.7038	2.6968	2.7497
	–	–	3.0386	2.9529	3.1685	2.7950
R(H···C)	–	–	–	–	3.0073	3.2833
THF No. 4	–	–	–	–	2.7013	2.7053
	–	–	–	–	2.7440	2.8026
	–	–	–	–	2.9639	2.8191
THF No. 1						
r(C–H)	1.1004	1.0100	1.0990	1.1014	1.1004	1.0992
Δr(C–H)	0.0009	−0.0895	−0.0005	0.0019	0.0009	−0.0003
r(C–H)	1.0991	1.0989	1.1001	1.0998	1.0998	1.0998
Δr(C–H)	−0.0004	−0.0006	0.0006	0.0003	0.0003	0.0003
r(C–H)	1.0999	1.0996	1.0997	1.1002	1.0989	1.0989
Δr(C–H)	0.0004	0.0001	0.0002	0.0007	−0.0006	−0.0006
r(C–H)	1.0992	1.1004	1.0991	1.1014	1.0961	1.1008
Δr(C–H)	−0.0003	0.0009	−0.0004	0.0019	−0.0034	0.0013
THF No. 2						
r(C–H)	1.1002	1.1007	1.1065	1.0993	1.1080	1.0993
Δr(C–H)	0.0007	0.0012	0.0070	−0.0002	0.0085	−0.0002
r(C–H)	1.0991	1.0996	1.1000	1.0991	1.1000	1.0996
Δr(C–H)	−0.0004	0.0001	0.0005	−0.0004	0.0005	0.0001
r(C–H)	1.0993	1.1001	1.1016	1.0999	1.1013	1.0989
Δr(C–H)	−0.0002	0.0006	0.0021	0.0004	0.0018	−0.0006
r(C–H)	1.0985	1.1010	1.0985	1.1006	1.1014	1.1011
Δr(C–H)	−0.0010	0.0015	−0.0010	0.0011	0.0019	0.0016

Table 2 (continued)

	THF dimer		THF trimer		THF tetramer	
Label	**A**	**B**	**A**	**B**	**A**	**B**
THF No. 3						
r(C–H)	–	–	1.1001	1.1004	1.1023	1.0994
Δr(C–H)	–	–	0.0006	0.0009	0.0028	−0.0001
r(C–H)	–	–	1.0994	1.0988	1.0996	1.1001
Δr(C–H)	–	–	−0.0001	−0.0007	0.0001	0.0006
r(C–H)	–	–	1.0993	1.0997	1.0994	1.0991
Δr(C–H)	–	–	−0.0002	0.0002	−0.0001	−0.0004
r(C–H)	–	–	1.1010	1.1004	1.0989	1.1011
Δr(C–H)	–	–	0.0015	0.0009	−0.0006	0.0016
THF No. 4						
r(C–H)	–	–	–	–	1.1008	1.0994
Δr(C–H)	–	–	–	–	0.0013	−0.0001
r(C–H)	–	–	–	–	1.0995	1.1000
Δr(C–H)	–	–	–	–	0.0000	0.0005
r(C–H)	–	–	–	–	1.0998	1.0990
Δr(C–H)	–	–	–	–	0.0003	−0.0005
r(C–H)	–	–	–	–	1.0976	1.1008
Δr(C–H)	–	–	–	–	−0.0019	0.0013

Bond lengths and binding energies ΔE are given in Å and kJ/mol, respectively. R(O···C) is the distance between the O atom from THF and the closest C atom from the SWCNT. R(H···O) is the distance between the H atom of the proton donor (THF) and the O atom of the proton acceptor (THF). The C-H···π hydrogen bonds are characterized by the R(H···C) distance between the H atom and the closest SWCNT carbon atom as well as the C-H bond length r(C-H) and its change with respect to the gas phase structure Δr(C-H)

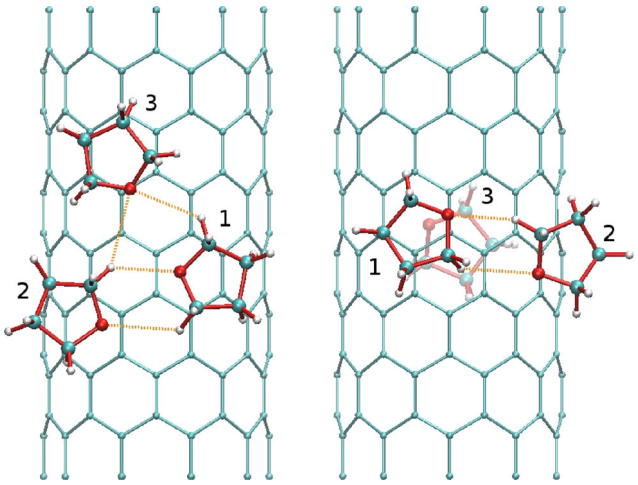

A : ΔE = − 92.6 kJ/mol (0.0) **B** : ΔE = − 88.9 kJ/mol (3.7)

Fig. 3 Global and local minima structures of THF trimers on SWCNT(10,0). The THF–THF interactions via C-H···O hydrogen bonds are marked by *dashed lines*. THF molecules are numbered for assignment of their structural parameters in Table 2. The relative binding energies are calculated with respect to the global minimum and are given in parenthesis

conformation C_2. Thus, in the THF trimer we observe the coexistence of molecules in the twisted and the envelope conformations. High-level ab initio calculations show that in the gas phase the global minimum of the THF trimer also consists of a mixture of C_s/C_2 conformations [22].

The structural trimer motif present in the global minimum **A** is larger than the THF dimer and therefore slightly sticks out from the curved surface of the carbon nanotube. The C-H···O hydrogen bonded network stabilizes the THF trimer and weakens one of the C-H···π hydrogen bonds, for which the H···C distance has become quite large, namely 4.5328 Å (see Table 2). If we calculate the contribution of the C-H···O hydrogen bonds to the trimer binding energy on the basis of the binding energy of the global minimum of the THF monomers, we obtain a very small value of only 5.3 kJ mol^{-1}. This is certainly an underestimation of the strength of the C-H···O hydrogen bond network, since we have assumed that all THF molecules in the trimer structure adopt the best possible position on the SWCNT surface. Due to the large size of the THF aggregate and the curvature of the nanotube, this is not the case, as evidenced by the increase of some of the H···C distances in the C-H···π hydrogen bonds, see Table 2.

All H···C and O···C intermolecular distances, which provide a measure for the structural adaption of the molecules on the surface, are summarized in Table 2. Except for the cases discussed above, all other structural parameters for the THF trimer structure **A** are close to those obtained for the THF monomer and dimer. Overall, as for the dimer, the dominant contribution to the binding energy originates from the sum of individual C-H···π hydrogen bonds. The observed changes in the C-H bond length Δr(C–H) suggest the existence of blue-shifting H-bonds of similar strength as in the THF dimer (see Adsorption of THF dimers on SWCNT(10,0)).

The trimer motif present in the global minimum **A** is dominated by the dimer. The ideal symmetric trimer configuration with all H-bonds being equivalent was not found as a stable local minimum. Structure **B** consists of the THF dimer known from the previous section and a THF monomer located on the other side of the SWCNT (see Fig. 3). The THF molecule number 3 has no contact with the THF dimer. As a result, structure **B** is less stable by 3.7 kJ mol^{-1} than the global minimum **A**. This shows that despite the curvature of the SWCNT, the THF molecules prefer to agglomerate and form clusters.

Adsorption of THF tetramers on SWCNT(10,0)

The analysis of the structural properties upon the addition of a fourth THF molecule to the THF trimer is the last step of our theoretical study. Since the THF molecule has only one oxygen atom serving as a proton acceptor site, the formation of larger symmetric aggregates on the surface of the carbon nanotube other than a tetramer is rather unlikely from a geometrical point of view. Larger symmetric arrangements of THF molecules would lead to some empty space in the center of the cluster and therefore such aggregates should be unstable at finite temperatures.

The construction of the initial THF tetramer configuration for the geometry optimization was inspired by the structural motif known as guanine quadruplex [53]. The guanine tetramer network is stabilized by cooperative weak N-H···O hydrogen bonds. Following this idea, we set up the so-called THF quad structure with four C-H···O hydrogen bonds where each THF is simultaneously a proton donor and a proton acceptor. Relaxation of the THF quad structures gives the global minimum **A** of the THF tetramer on the surface with a binding energy of −147.8 kJ mol^{-1}, see Fig. 4. The strength of the cooperative network of four C-H···O hydrogen bonds in the THF quad is estimated by subtracting four times the binding energy of the THF monomer **A** from the binding energy of the THF quad. The obtained value for the full network of four C-H···O hydrogen bonds is 29.0 kJ mol^{-1}, so the contribution of each H-bond is about 7 kJ mol^{-1}. This is significantly larger than

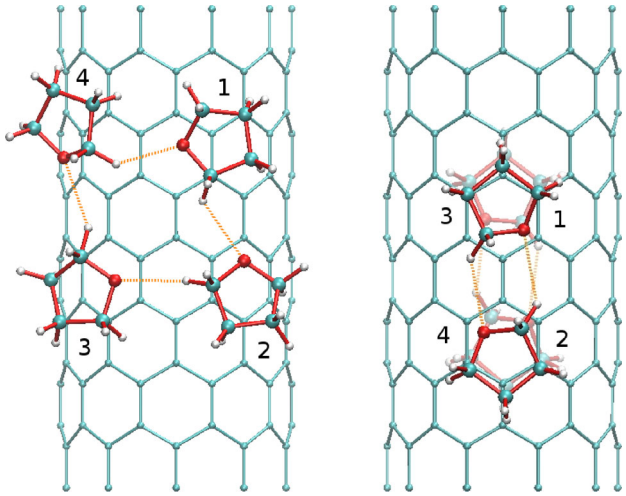

A : ΔE = − 145.4 kJ/mol (0.0) **B** : ΔE = − 129.6 kJ/mol (15.8)

Fig. 4 Global and local minima structures of THF tetramers on SWCNT(10,0). The THF–THF interactions via C-H···O hydrogen bonds are marked by *dashed lines*. THF molecules are numbered for assignment of their structural parameters in Table 2. The relative binding energies are calculated with respect to the global minimum and are given in parenthesis

the value estimated for the global minimum structure of the THF dimer, which was 3 kJ mol^{-1} (see Adsorption of THF dimers on SWCNT(10,0)).

The cooperative network of four cyclic C-H···O hydrogen bonds in the THF quad structure results in a larger contribution of the solvent–solvent interactions to the binding energy than for the THF dimer. This energetic effect might be explained by an analysis of the structural parameters of the C-H···O hydrogen bonds (see Table 2). The values of the H···O distances in the THF quad structure are shorter than those in the THF dimer or trimer. Additionally, some of the C-H bonds involved in the H-bonds are significantly contracted, for example, in the THF molecule number 4 Δr(C–H) is −0.0034 Å. According to the correlations mentioned in "Adsorption of THF monomers on SWCNT(10,0)", the blue-shift in this case is predicted to be of the order of 50 cm^{-1}. The estimated strength of a single C-H···O bond in the global minimum structure of the THF tetramer suggests that THF molecules on the SWCNT surface rather form quads and not the dimer motif. On the other hand, the strength of the C-H···π hydrogen bonds in the THF quad structure, estimated on the basis of the values of the H···C distance, is similar to that obtained for THF monomer, dimer or trimer (see Table 2). By high-level ab initio calculations it was shown that THF tetramers in the gas phase consist of THF molecules in both C_s and C_2 configuration [22]. In the global minimum structure of the THF quad on the surface we observe the same behavior: molecule number 2 and 3 are in the C_2 and molecule number 1 and 4 are in the C_s configuration.

Structure **B** was constructed as a reference configuration to further elucidate the strength of the cooperative network of four C-H$\cdots$O hydrogen bonds in the THF quad structure (see Fig. 4). Local minimum **B** consists of two THF dimers adsorbed on opposite sides of the SWCNT(10,0). It is less stable by 15.8 kJ mol^{-1} than the global minimum **A**. The diameter of the SWCNT(10,0) is almost 8 Å, therefore the two THF dimers in structure **B** do not interact with each other. The binding energy difference between the THF tetramers **A** and **B** can be then attributed to the two missing C-H$\cdots$O hydrogen bonds in THF tetramer **B**. The structural parameters (O$\cdots$C, H$\cdots$O and H$\cdots$C distances) obtained for THF tetramer structure **B** are similar to those for the THF dimers (see Table 2). According to our results from "Adsorption of THF monomers on SWCNT(10,0)" it is not surprising that all molecules in structure **B** are in their global minimum envelop C_s configuration.

Finally, Car–Parrinello molecular dynamics (CP-MD) simulations were performed to explore the dynamical reaction pathways for structural rearrangements of THF molecules on the SWCNT(10,0) surface at finite temperatures. Furthermore, the CP-MD simulations were used to validate the stability of the THF dimer and tetramer structures at room temperature. Experimental studies based on neutron scattering have shown the existence of a predominantly T-like packing of the THF molecules in the liquid phase [24]. Our CP-MD simulations will shed some light on this issue.

Figure 5 shows the time evolution of the THF tetramer structure on the SWCNT(10,0) surface at 300 K. The corresponding time of the snapshots from the CP-MD simulation is given in each frame. It is not possible to show in detail all bond-breaking and bond-formation events. The selected snapshots only refer to general changes in the structural motif of the THF tetramer with special focus on the pseudorotation issue. The initial configuration for the CP-MD run was the global minimum of the THF tetramer (see structure **A** in Fig. 4). However, the quad

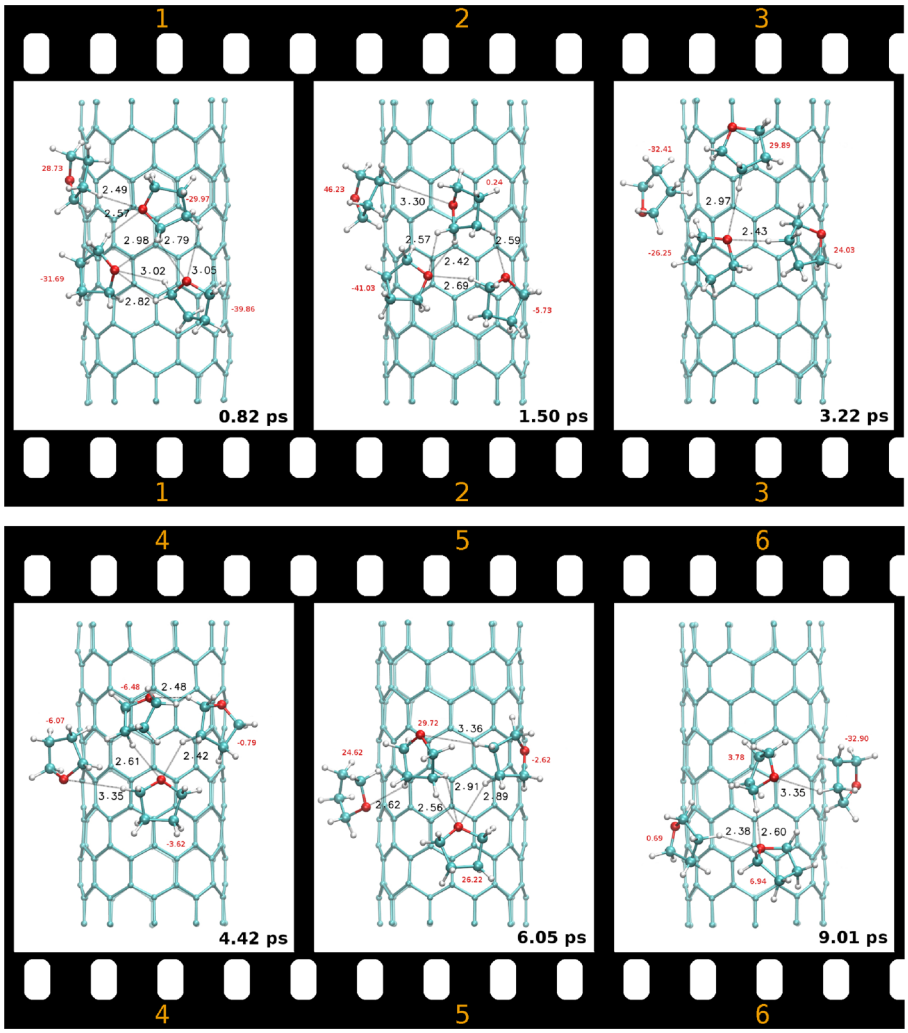

Fig. 5 Snapshots from one selected CP-MD simulation of a THF tetramer on SWCNT(10,0) at 300 K. Each snapshot is labeled by the time when it was taken from the trajectory. *Red and black labels* refer to the pseudorotation angle ϕ and the intermolecular bonds, respectively

structure undergoes a molecular rearrangement already in the equilibration phase, therefore this structural motif is no longer present at the beginning of the production run.

The structure from the first snapshot in Fig. 5 consists of the THF dimer motif with two parallel C-H···O hydrogen bonds surrounded by two other THF molecules. Each oxygen atom in the THF molecules from the dimer acts as the proton acceptor for two C-H···O hydrogen bonds. The value of the pseudorotation angle ϕ, namely the C-C-C-C dihedral angle, is given next to each THF molecule (see Fig. 5). The pseudorotation angle ϕ in the THF molecule is associated with the ring conformation. Values close to zero refer to a coplanarity of four adjacent ring carbon atoms (i.e., the envelope C_s conformation), whereas values of about ±30 degrees indicate coplanarity of three adjacent ring carbon atoms and the midpoint between the opposite bond (i.e., the twisted C_2 conformation) [19]. At the time of the first snapshot at 0.82 ps, all THF molecules are in the twisted configuration C_2. The time evolution of the pseudorotation angle ϕ for the entire production run is shown in Fig. 6. The conformational motif from the first snapshot in Fig. 5 is stable for about 0.3 ps. Then it undergoes changes and as a result two THF molecules adapt the global minimum structure C_s (see the changes of the pseudorotation angle ϕ at 1 ps in Fig. 6). Many more of these structural rearrangements occur during the 10-ps-long MD trajectory. Due to their large number, it is not possible to discuss all of them in detail.

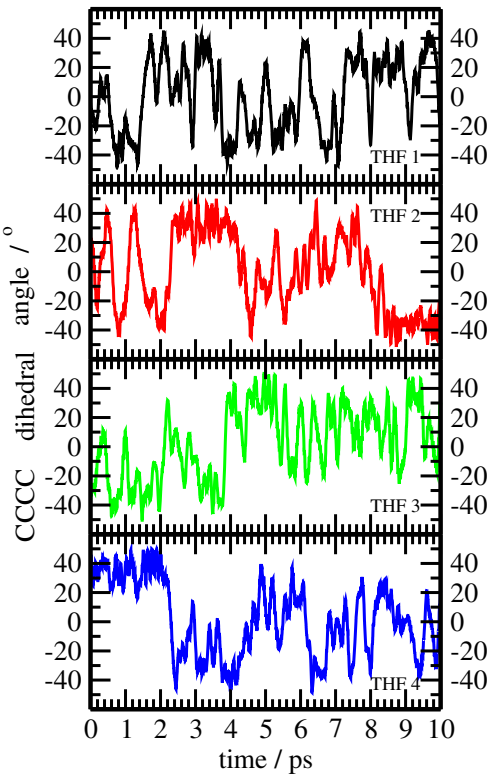

Fig. 6 The time evolution of the pseudorotation angle ϕ in the CP-MD simulation of a THF tetramer on SWCNT(10,0) at 300 K. Each color refers to one THF molecule in the THF tetramer on the surface

The second snapshot in Fig. 5 shows the structural motif at the time of 1.50 ps. The THF dimer is no longer present, instead some distorted THF trimer appears. The fourth THF molecule is somewhat detached from the trimer with a H···O distance of 3.30 Å. Here, the C-H···O hydrogen bonds in the trimer are quite strong. The H···O distances vary from 2.42 to 2.69 Å. Two molecules in the trimer are in their global minimum envelop structure C_s, whereas the third one has the twisted configuration C_2. The estimated lifetime of the C_s configuration (see Fig. 6) is very short (tens of fs). The THF molecules in the C_s configuration are very labile and easily transform into C_2 structure. The oscillations of the pseudorotation angle ϕ are visible in Fig. 6, see for example the red curve in the time range from 0 to 2 ps. The estimated time for the full THF rearrangement from the global minimum C_s to a conformation with positive or negative value of the pseudorotation angle ϕ and then back to the initial C_s configuration is about 1 ps. Other patterns are also observed where THF molecules stay for a longer time (1–2 ps) in the twisted configuration C_2 due to the their mutual interactions.

The third snapshot in Fig. 5 shows the THF tetramer structure at the time of 3.22 ps. The molecular arrangement changes rapidly and the THF trimer motif is no longer present. All THF molecules are in the twisted configuration C_2 and only two C-H···O hydrogen bonds are observed. The oxygen atom from one THF molecule serves as proton acceptor for C-H···O hydrogen bonds with two other, non-interacting THF molecules. No C-H···O hydrogen bonds between these three THF and the remaining fourth THF molecule are observed.

After 1.2 ps, the bonding pattern has changed again. The two THF molecules, previously non-interacting, change their configuration to the envelope C_s and form a strong C-H···O hydrogen bond, with a H···O distance of 2.48 Å, see the fourth snapshot in the Fig. 5). The other two THF molecules are also in the envelope configuration. Thus, within a period of 1.2 ps we observe a cooperative action where all THF molecules change simultaneously their conformation from C_2 to C_s. This conformational change takes only about 0.2 ps and is steered by the formation of the new C-H···O hydrogen bonded network.

The fifth snapshot in Fig. 5 shows the THF tetramer structure at the time of 6.05 ps. Three THF molecules are in the C_2 configuration. The observed structural THF trimer motif resembles that from the third snapshot. The oxygen atom from one THF molecule serves as a double proton acceptor for the C-H···O hydrogen bonds with two non-interacting THF molecules. The difference between the structures at 6.05 ps (5th snapshot) and 3.22 ps (3rd

snapshot) is that at 3.22 ps the fourth THF molecule forms a C-H$\cdots$O hydrogen bond to one THF in the trimer (the H$\cdots$O distance is 2.62 Å).

The last snapshot in Fig. 5 at 9.01 ps shows the formation of a structure with some structural motifs similar to those observed in the calculations for the THF aggregates in the gas phase [22]. One of the THF molecules interacts with the carbon nanotube only via βC-H$\cdots\pi$ hydrogen bonds, so the plane spanned by the carbon skeleton of the THF molecule is perpendicular to the SWCNT surface. This molecule forms a αC-H$\cdots$O hydrogen bond with the neighboring molecule with a H$\cdots$O distance of 2.60 Å. Such a T-like packing motif of the THF molecules exists predominantly in the liquid phase [24]. The underlying trimer motif in the T-like structure is the result of a previously observed rearrangement of the tetramer (see the fifth snapshot in Fig. 5).

In summary, complex scenarios of many bond-breaking and bond-formation events are observed. It is therefore not possible to analyze all individual molecular rearrangements in detail and we have focused only on the most important transformations.

Conclusions

The structure of THF_{1-4} aggregates on the surface of a (10,0) single-walled carbon nanotube was analyzed by DFT geometry optimizations and Car–Parrinello molecular dynamics simulations. A stepwise increase of the SWCNT surface coverage by adding THF molecules, starting from the monomer, via dimer and trimer and ending at the tetramer, enabled an extensive study of a potential energy surface with many local energy minima structures. All structures were analyzed in terms of solvent–solvent (THF–THF) and solvent–surface (THF–SWCNT) interactions via C-H$\cdots$O and C-H$\cdots\pi$ hydrogen bonds, respectively. The binding energies of the THF dimer, trimer, and tetramer are dominated by C-H$\cdots\pi$ hydrogen bonded interactions. However, the calculated contribution from the C-H$\cdots$O hydrogen bonds to the binding energy is also important. The character of the H-bonds in the THF/SWCNT(10,0) structures was determined based on the correlations between the change of the C-H bond length and the shift of the ν(CH) stretching vibration. By this analysis, improper, blue-shifting H-bonds of different strength were found. The results of the static DFT calculations at 0 K suggest that the THF quad structure is the most stable among all THF_{1-4} aggregates and should be more abundant than the THF dimer motif. However, the CP-MD simulations of the quad structure performed at 300 K show its instability. The tetramer structure is very labile on the surface and the H-bonded network undergoes a complicated evolution, therefore many bond-breaking and bond-formation events were observed. The structural rearrangements are correlated with the pseudorotation of the THF carbon skeleton. A cleavage/formation of the C-H$\cdots$O hydrogen bonds influences the changes of the C_s/C_2 configuration of THF molecules. It is often a cooperative movement where all THF molecules changed simultaneously their conformation. Contrary to the THF quad structure, the THF dimer motif was indeed found at the finite temperature of the CP-MD simulations. The C-H$\cdots$O hydrogen bonds in the dimer are also very labile due to the mutual interactions with the neighboring THF molecules. The lifetime of a THF dimer bond was only about 1 ps. Altogether, the observed changes of the structural motifs of the THF_{1-4} aggregates on the surface suggest the prevalence of the C-H$\cdots\pi$ over C-H$\cdots$O hydrogen bonds.

Acknowledgments This work was supported by the Foundation for Polish Science (FNP) within the HOMING PLUS programme and the German Research Foundation (DFG) within the Collaborative Research Center SFB 953 “Synthetic Carbon Allotropes”. Computational resources were provided by BOVILAB@RUB (Bochum) and RRZE (Erlangen).

References

1. Sgobba V, Guldi DM (2009) Chem Soc Rev 38:165
2. Hirsch A (2010) Nat Mater 9:868
3. Dillon AC (2010) Chem Rev 110:6856
4. Karousis N, Tagmatarchis N, Tasis D (2010) Chem Rev 110:5366
5. Hirsch A (2002) Angew Chem 41:1853
6. Geckeler KE, Premkumar T (2011) Nanoscale Res Lett 6:136
7. Desiraju GR, Steiner T (1999) The weak hydrogen bond: in structural chemistry and biology. Oxford University Press, New York
8. Kozlowska M, Rodziewicz P, Utesch T, Mroginski MA, Kaczmarek-Kedziera A (2018) Phys Chem Chem Phys 20:8629
9. Pimentel GC, McClellan AL (1971) Ann Rev Phys Chem 21:347
10. Scheiner S (1997) Hydrogen bonding. Oxford University Press, New York
11. Kozlowska M, Goclon J, Rodziewicz P (2016) ChemPhysChem 17:1143
12. van der Veken BJ, Herrebout WA, Szostak R, Shchepkin DN, Havlas Z, Hobza P (2001) J Am Chem Soc 123:12290
13. Kumar RM, Elango M, Subramanian V (2010) J Phys Chem A 114:4313
14. Donoso-Tauda O, Jaque P, Santos JC (2011) Phys Chem Chem Phys 13:1552
15. Tasis D, Tagmatarchis N, Bianco A, Prato M (2006) Chem Rev 106:1105
16. Wang D, Lu S, Jiang SP (2010) Electrochim Acta 55:2964

17. Cadioli B, Gallinella E, Coulombeau C, Jobic H, Berthier G (1993) J Phys Chem 97:7844
18. Strajbl M, Florian J (1998) Theor Chem Acc 99:166
19. Meyer R, López JC, Alonso JL, Melandri S, Favero PG, Caminati W (1999) J Chem Phys 111:7871
20. Melnik DG, Gopalakrishnan S, Miller TA, Lucia FCD (2003) J Chem Phys 118:3589
21. Rayon VM, Sordo JA (2005) J Chem Phys 122:204303
22. Boese AD, Boese R (2015) Cryst Growth Des 15:1073
23. Yang T, Su G, Ning C, Deng J, Wang F, Zhang S, Ren X, Huang Y (2007) J Phys Chem A 111:4927
24. Bowron DT, Finney JL, Soper AK (2006) J Am Chem Soc 128:5119
25. Chandrasekhar J, Jorgensen WL (1982) J Chem Phys 77:5073
26. Giambiagi MS, Neto MO, Neder AVF (2005) J Math Chem 38:519
27. Grabowski SJ, Leszczynski J (2009) Chem Phys 355:169
28. Stanca-Kaposta EC, Gamblin DP, Screen J, Liu B, Snoek LC, Davis BG, Simons JP (2007) Phys Chem Chem Phys 9:4444
29. Kozmon S, Matuska R, Spiwok V, Koca J (2011) Phys Chem Chem Phys 13:14215
30. Kumar RM, Baskar P, Balamurugan K, Das S, Subramanian V (2013) RSC Adv 3:7798
31. Kumar M, Balaji PV (2014) J Mol Model 20:2136
32. Hedman D, Barzegar HR, Rosén A, Wågberg T, Larsson JA (2015) Sci Rep 5:16850
33. Giannozzi P, Baroni S, Bonini N, Calandra M, Car R, Cavazzoni C, Ceresoli D, Chiarotti GL, Cococcioni M, Dabo I, Corso AD, de Gironcoli S, Fabris S, Fratesi G, Gebauer R, Gerstmann U, Gougoussis C, Kokalj A, Lazzeri M, Martin-Samos L, Marzari N, Mauri F, Mazzarello R, Paolini S, Pasquarello A, Paulatto L, Sbraccia C, Scandolo S, Sclauzero G, Seitsonen AP, Smogunov A, Umari P, Wentzcovitch RM (2009) J Phys Condens Matter 21:395502
34. Perdew JP, Burke K, Ernzerhof M (1996) Phys Rev Lett 77:3865
35. Vanderbilt D (1985) Phys Rev B 32:8412
36. Grimme S (2006) J Comp Chem 27:1787
37. Frey JT, Doren DJ (2011) TubeGen 3.4 (web-interface, http://turin.nss.udel.edu/research/tubegenonline.html). University of Delaware, Newark
38. Car R, Parrinello M (1985) Phys Rev Lett 55:2471
39. Hutter J, Ballone P, Bernasconi M, Focher P, Fois E, Goedecker S, Marx D, Parrinello M, Tuckerman M CPMD 3.17
40. Nosé S (1984) J Chem Phys 81:511
41. Hoover WG (1985) Phys Rev A 31:1695
42. VandeVondele J, Krack M, Mohamed F, Parrinello M, Chassaing T, Hutter J, Comput J (2005) Phys Commun 167:103
43. Rodziewicz P, Melikova SM, Rutkowski KS, Buda F (2005) ChemPhysChem 6:1719
44. Rodziewicz P, Melikova SM, Rutkowski KS, Koll A, Buda F (2006) ChemPhysChem 7:1221
45. Rodziewicz P, Rutkowski KS, Meyer B (2011) Phys Chem Chem Phys 13:14101
46. Rodziewicz P, Meyer B (2014) Phys Chem Chem Phys 16:940
47. Woods LM, Bădescu SC, Reinecke TL (2007) Phys Rev B 75:155415
48. Kryachko ES, Zeegers-Huyskens T (2001) J Phys Chem A 105:7118
49. Fan JM, Liu L, Guo QX (2002) Chem Phys Lett 365:464
50. Zierkiewicz W, Jurecka P, Hobza P (2002) ChemPhysChem 6:609
51. Gu Y, Kar T, Scheiner S (1999) J Am Chem Soc 121:9411
52. Qian W, Krimm S (2002) J Phys Chem A 106:6628
53. Mergny JL, Helene C (1998) Nat Med 4:1366